Journal of Applied Fluid Mechanics, Vol. 17, No. 5, pp. 939-950, 2024.
Available online at www.jafmonline.net, ISSN 1735-3572, EISSN 1735-3645.
https://doi.org/10.47176/jafm.17.05.2340

Numerical Simulations of Turbulent Gas-solid Flow in a Gradual Expansion

A. Benavides-Moran[1†] and S. Lain[2]

[1] *Department of Mechanical and Mechatronics Engineering, Universidad Nacional de Colombia, sede Bogotá, Colombia*
[2] *Department of Mechanical Engineering. Universidad Autónoma de Occidente, 760030 Cali, Colombia*

†Corresponding Author Email: agbenavidesm@unal.edu.co

ABSTRACT

Modeling efforts on turbulent gas-solid flows have mainly focused on studying particle-laden flows in channels and pipes. Despite its significance for industrial applications, the study of gas-solid flows in sudden or gradual expansions is less common in the literature. This paper challenges current two-phase flow models to compute the dilute turbulent gas-solid flow in a vertically oriented 12° conical diffuser. The solids phase is modeled in two ways: the Two-Fluid Model approach that incorporates closure relations derived from the kinetic theory of granular flow, and the Euler-Lagrange particle tracking model with two-way coupling. In both cases, turbulence in the gas phase is estimated by the Reynolds stress model with additional modulation terms that account for the effect of the particles on the gas-phase turbulence. Simulation results are validated versus experimental benchmark data not only for gas axial velocity but also for streamwise and radial turbulence intensity, as comparison with such turbulent variables has not been detailed in previous studies. Nevertheless, due to the lack of experimental data for validation, profiles of solids axial velocity are only compared numerically. Contours of turbulence kinetic energy and granular temperature in the diffuser region reveal a high shear area responsible for the production of turbulence in both phases. Moreover, results obtained from the Euler-Lagrange model show an intense particle fluctuating velocity in the streamwise direction downstream of the diffuser.

Article History

Received September 26, 2023
Revised November 14, 2023
Accepted December 4, 2023
Available online February 24, 2024

Keywords:

Two-fluid model
Kinetic theory of granular flow
Two-way coupling
Turbulence modulation
Ansys-Fluent

1. INTRODUCTION

Turbulent carrier fluids with suspended small solid particles are commonly found in industrial applications. An in-depth understanding of how the carrier fluid (gas phase) and the particles (solids phase) behave under varying conditions is essential for the effective design and reliable operation of industrial systems, such as in the case of pneumatic conveying of particulate matter. However, little attention has been given to the gas-solid flow in continuous pipe expansions in which boundary layer separation effects play a major role. Experimental observations show that particles can reduce or even eliminate flow separation in a diffuser. Kale and Eaton (1985) experimentally investigated the gas-solid flow through diffusers of various configurations; they found that suspended particles exert a drag on the gas which results in a more favorable pressure gradient in the diffuser section. The flow pattern in circulating fluidized bed (CFB) risers is significantly affected by the presence of a diffuser. Schut et al. (2000) observed strong re-circulation of particles when the oncoming flow exhibited a core-annulus structure. The downflow of solids was found to be particularly intense at the diffuser outlet. This may present an advantage in terms of longer residence times in CFB risers.

The main approaches to simulate turbulent gas-solid flows in channels and pipes differ on the choice of turbulence modeling and the way in which the solids phase is treated. Most numerical works adopt the *Eulerian-Lagrangian* (EL) framework in which the gas phase can be modeled by DNS (Direct Numerical Simulation), LES (Large-Eddy Simulation) or RANS (Reynolds-Average Navier-Stokes) equations while the solids phase is represented by a finite number of particle parcels whose motion is tracked by solving Newton's second law (Laín et al., 2002). Triesch and Bohnet (2001) extended the E-L model in the commercial CFD software Fluent to account for the influence of wall

NOMENCLATURE

C_D	drag coefficient	$\vec{v}$	velocity fluctuation
C_p	pressure recovery coefficient	$\vec{V}$	mean velocity
d_s	particle mean diameter	$\vec{V}_{dr}$	drift velocity
D	pipe diameter	x	Streamwise coordinate
$\mathcal{D}_{sg}$	turbulent dispersion coefficient	α	opening angle
e	restitution coefficient	β_{sg}	interphase momentum transfer coefficient
$\vec{F}_{td}$	turbulent dispersion force	γ_s	collisional dissipation
$\vec{g}$	acceleration due to gravity	ϵ	Dissipation rate
g_0	radial distribution function	Θ_s	granular temperature
$\mathcal{I}$	identity tensor	κ_s	solids conductivity
k	turbulent kinetic energy	λ_s	solids bulk viscosity
k_{sg}	gas-solids fluctuating velocity covariance	μ	viscosity
L	length	Π	turbulence modulation term
p	pressure fluctuation	ρ	density
P	mean pressure field	τ	characteristic time scale
r	radial coordinate	φ	specularity coefficient
R	pipe radius	ϕ	volume fraction
$\mathcal{R}_g$	Reynolds stress tensor	**Subscripts**	
t	time	g	gas phase
$\mathcal{T}$	stress tensor	s	solids phase
u′	streamwise turbulent intensity	t	turbulent
v′	radial turbulent intensity	w	wall

roughness on particle-wall collisions; their E-L model also included the Magnus lift force and the extended Saffmann lift force. Mean particle velocity and solids volume concentration profiles showed good agreement with experimental data for a solids loading of one. De Souza et al. (2014) adopted the EL approach to computing the gas-solid flow in a vertical conical diffuser. Their approach included four-way coupling and wall roughness effects. Simulation results showed a significant decrease in flow separation within the diffuser even at low mass loading ratios. El-Askary et al. (2015) implemented an axisymmetric two-phase flow model within the EL framework to investigate the effect of the opening angle on the diffuser performance. The hard sphere collision model was implemented to account for particle-particle and particle-wall interactions. Computations were performed on a cartesian grid which approximated the diffuser boundary as staircase-like steps. Their results showed that the size of the separation zone is reduced for particle-laden flow through a 7° conical diffuser. The size of the separation seemed to be reduced as the inlet Reynolds number and solid mass flow rate increased.

The *Eulerian-Eulerian* framework treats the solid phase as a continuous medium with properties analogous to those of a real fluid. This approach is also known as the Two-Fluid Model (TFM). The assumption of fluid-like behavior for the solids phase leads to a closure problem as the solids phase stress tensor, the interphase momentum transfer term, the particle-wall boundary condition, and turbulence modulation need to be specified (Benavides & van Wachem, 2009). Senapati and Dash (2021) used the TFM to study the hydrodynamics and pressure recovery of dilute gas-solid flow in a conical diffuser. The computational domain was axisymmetric and it was discretized with less than 32000 cells. They found that the choice of specularity coefficient (the fraction of momentum conserved after a particle collides with a wall) and the interparticle restitution coefficient affect the estimated pressure recovery and strength of the flow recirculation zone in the diffuser. They noticed that the reverse momentum transfer mechanism is weakened for high values of the specularity coefficient (about 0.8) and restitution coefficients less than 0.95.

The purpose of this work is to perform a numerical investigation of the turbulent gas-solid flow in a vertically oriented conical diffuser as it is described by Bohnet and Triesch (2003) for glass spheres of 150 μm in diameter and mass loading ratio of 0.5. The TFM and the EL implemented in the commercial CFD software ANSYS-Fluent version 2022-R2 are used to describe the dynamics of the solids phase and the results compared with the experimental measurements of Bohnet and Triesch (2003). To the best of our knowledge, this is the first time in which TFM simulations are compared with this specific set of experiments. Moreover, attention is focused on the influence of the solids phase modeling on the predictions of streamwise and radial turbulence intensity, which is a subject not fully addressed in previous investigations. Finally, the diffuser performance based on the pressure recovery coefficient is also estimated for single-phase and two-phase flows.

2. MATHEMATICAL MODELS

The ability of a diffuser to convert the kinetic energy of a fluid into pressure energy is determined by the pressure recovery coefficient:

$$C_p = \frac{\Delta p}{\rho V_{inlet}^2/2} \tag{1}$$

Where Δp is the difference in static pressure through the diffuser. The ideal value of C_p depends only on the inlet-to-outlet area ratio. The diffuser loss coefficient is the difference between actual and ideal values of C_p; empirical correlations have been proposed to estimate the diffuser loss coefficient and can be found in (Rennels and Hudson, 2012). The pressure recovery coefficient is expected to be affected by the presence of the solids phase, something that is assessed in this work.

2.1 The Two-Fluid Model

The Eulerian-Eulerian or Two-Fluid Model approach treats the solid phase as a continuum with transport equations similar to those of a fluid. In the TFM, the conservation equations for the gas phase incorporate the effect of the particles on the fluid flow. The continuity equation for the gas phase is:

$$\frac{\partial}{\partial t}\left(\phi_g \rho_g\right) + \nabla \cdot \left(\phi_g \rho_g \vec{V}_g\right) = 0 \tag{2}$$

Where volume conservation requires that gas and solid volume fraction sum up to unity, i.e. $\phi_g + \phi_s = 1$. In this work, the drag proportional to the mean relative velocity $\left(\vec{V}_g - \vec{V}_s\right)$ is assumed to be the dominant force; the momentum equations also include a force term ($\vec{F}_{td}$) that accounts for particle dispersion by the fluid turbulent motion:

$$\frac{\partial}{\partial t}\left(\phi_g \rho_g \vec{V}_g\right) + \nabla \cdot \left(\phi_g \rho_g \vec{V}_g \vec{V}_g\right) = -\phi_g \nabla P +$$

$$\phi_g \nabla \cdot \left(\mathcal{T}_g + \rho \mathcal{R}_g\right) + \phi_g \rho_g \vec{g} - \beta_{sg}\left(\vec{V}_g - \vec{V}_s\right) + \vec{F}_{td} \tag{3}$$

Where $\vec{V}_g$ is the gas phase mean velocity and P is the mean pressure field shared by both phases. The interphase momentum transfer coefficient, β_{sg}, is modeled according to Wen & Yu (1966); this correlation was experimentally determined from the settling of solid particles in a liquid over a wide range of solids volume fractions. Constitutive relations derived from kinetic theory of granular flow (KTGF) can be used to represent the solids phase stresses at low and moderate volume solids phase volume fraction (dilute flow). Terms such as the solids pressure (P_s) and shear stress tensor ($\mathcal{T}_s$) consider particle-particle interactions (collisions) and fluid-induced particle fluctuations in the momentum conservation equation for the solids phase:

$$\frac{\partial}{\partial t}\left(\phi_s \rho_s \vec{V}_s\right) + \nabla \cdot \left(\phi_s \rho_s \vec{V}_s \vec{V}_s\right) = -\phi_s \nabla P - \nabla P_s +$$

$$\nabla \cdot \mathcal{T}_s + \phi_s \rho_s \vec{g} + \beta_{sg}\left(\vec{V}_g - \vec{V}_s\right) - \vec{F}_{td} \tag{4}$$

The Reynolds Stress Model (RSM) is chosen to account for turbulence in the gas phase. Turbulent diffusion and pressure strain terms in the RSM are described according to the single-phase turbulence modeling; standard terms in the RSM include the gas phase volume fraction (ϕ_g) which is close to unity for dilute gas-solid flows. Turbulence modulation terms are included in the transport equations for the Reynolds stresses ($\mathcal{R}_g$) and the dissipation rate (ϵ):

$$\frac{\partial}{\partial t}\left(\phi_g \rho_g \mathcal{R}_g\right) + \nabla \cdot \left(\phi_g \rho_g \vec{V}_g \mathcal{R}_g\right) =$$

$$-\phi_g \rho_g \left[\mathcal{R}_g \cdot \nabla \vec{V}_g + \left(\mathcal{R}_g \cdot \nabla \vec{V}_g\right)^T\right] +$$

$$\phi_g \nabla \cdot \left(\mu_g \mathcal{R}_g\right) - \nabla \cdot \left(\phi_g \rho_g \overline{\vec{v}_g \vec{v}_g \vec{v}_g}\right) +$$

$$\phi_g \overline{p\left[\nabla \vec{v}_g + \left(\nabla \vec{v}_g\right)^T\right]} - \frac{2}{3}\left(\phi_g \rho_g \epsilon - \Pi_k\right)\mathcal{I} \tag{5}$$

$$\frac{\partial}{\partial t}\left(\phi_g \rho_g \epsilon\right) + \nabla \cdot \left(\phi_g \rho_g \vec{V}_g \epsilon\right) = \nabla \cdot \left[\phi_g \left(\mu_g + \frac{\mu_t}{\sigma_\epsilon}\right)\nabla \epsilon\right] +$$

$$\phi_g \rho_g \left[C_{\epsilon,1} \mathcal{R}_g : \nabla \vec{V}_g - C_{\epsilon,2}\epsilon + \Pi_\epsilon\right] \tag{6}$$

The term Π_k in Eq. (5) couples the fluctuating motion in the gas and solid phases; it is a turbulence modulation term that approximates the turbulence enhancement or attenuation due to the presence of particles. The term Π_ϵ in Eq. (6) is proportional to Π_k. The solid phase pressure and shear stress tensor are related to the pseudo-thermal energy or granular temperature (Θ_s); a transport equation for granular temperature (turbulence kinetic energy in the solid phase) is incorporated in the TFM to account for the transfer of momentum and energy as a result of particle random motion:

$$\frac{3}{2}\left[\frac{\partial}{\partial t}\left(\phi_s \rho_s \Theta_s\right) + \nabla \cdot \left(\phi_s \rho_s \vec{V}_s \Theta_s\right)\right] = \nabla \cdot \left(\kappa_s \nabla \Theta_s\right) +$$

$$\left(-P_s \mathcal{I} + \mathcal{T}_s\right) : \nabla \vec{V}_s - \gamma_s - 3\beta_{sg}\Theta_s \tag{7}$$

Turbulence kinetic energy in the solids phase is directly generated by shear, or indirectly by fluid turbulence and particle interactions. It dissipates by collisions (γ_s is modeled according to Lun et al. (1984)) or due to the effect of drag on the particle fluctuations (LaMarche et al., 2017). Constitutive relations for the solids phase derived from the KTGF, such as the solids pressure, P_s, and bulk viscosity proposed by Lun et al. (1984), the shear viscosity and conductivity (Syamlal et al., 1993), and the radial distribution function derived by (Sinclair & Jackson, 1989) are found in Table A1 (Appendix). The turbulence modulation closures adopted by Viollet and Simonin (1990) for the covariance of gas phase and solid phase velocity fluctuation, k_{sg}, and drift velocity are found in Table A2 (Appendix).

2.2 The Eulerian-Lagrangian Model

In the Eulerian-Lagrangian (EL) framework, the motion of individual particles is traced by solving Newton's second law. A significant number of computational particles needs to be tracked to characterize the dynamics of the solids phase. For this reason, the EL model is applicable to dilute particle-laden flows such as the one studied in this work.

In this study, the EL computations, as well as the TFM, have been performed using the RSM for describing the turbulent behavior of the gas phase (Eq. (5)). The pressure-strain term has been modeled by the Linear Pressure Strain (LPS) model considering wall reflection effects (Speziale, 1995; Ansys, 2022). The wall boundary conditions from turbulent kinetic energy, k, have been employed using an enhanced wall treatment (Ansys,

2022). As a first approach, the forces considered in the particle evolution equation have been the drag and weight-buoyancy contributions, disregarding lift forces. The roughness of the wall has been considered in particle-wall interactions, according to the model implemented in Fluent (Ansys, 2022). A small roughness has been considered in this work with an rms angle of virtual wall inclination of 1.9 degrees (De Souza et al., 2014). Normal and tangential restitution coefficients for particle inelastic rebound against the wall are equal to 0.95.

The description of the particle-laden flow in the diffuser considered the two-way coupling, i.e. effects of the dispersed phase on the continuous one, but owing to the dilute conditions ($\phi_{s,inlet} = 2.45 \times 10^{-4}$) inter-particle collisions have been disregarded (Crowe et al., 2011). This choice also allowed to keep simulation times affordable in the available hardware. Here, around a million parcels have been tracked in the flow field. Coupling between the phases has been described by the Particle Source in Cell (PSIC) approach (Laín & Sommerfeld, 2007, 2013). Finally, according to De Souza et al. (2014), the source terms for the Reynolds Stress components and its dissipation rate were not considered in the Euler-Lagrange simulations performed in this work. Omitting such source terms is not anticipated to impact the results due to the low particle Reynolds numbers and volume fraction.

3. COMPUTATIONAL METHODOLOGY

A schematic of the computational domain is shown in Fig. 1 and its dimensions are summarized in Table 1. The fully three-dimensional computational domain was discretized into 4 million hexahedral cells which was found to provide grid-independent results (see section 3.2). As it can be seen in Table 1, the inlet pipe is long enough to ensure fully-developed flow at the diffuser inlet.

3.1 Simulation Setup

The numerical solver parameters used by the TFM are summarized in Table 2. A coupled solver together with high-order schemes was used throughout the iterative process. The specified under-relaxation factors for body forces, volume fraction, turbulence quantities, Reynolds stresses, and granular temperature were 0.5, 0.5, 0.8, 0.5, and 0.3 respectively. All flow quantities satisfy the same convergence criterion at every time step.

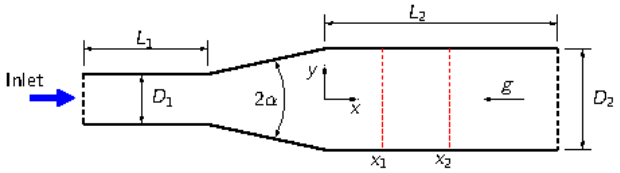

Fig. 1 Simplified computational domain of the conical diffuser. Relevant dimensions are shown in Table 1. Profiles are plotted at the downstream positions $x_1 = 0.7$ m and $x_2 = 2.2$ m

Table 1 Dimension, fluid and particle properties, and flow parameters

Parameter	Value
Diffuser	
Inlet diameter, D_1	29 mm
Outlet diameter, D_2	52.3 mm
Opening angle, α	6°
Length of pipe before diffuser, L_1	5 m
Length of pipe behind diffuser, L_2	9 m
Solids phase	
Particle mean diameter, d_s	150 μm
Particle density, ρ_s	2500 kg/m^3
Gas phase	
Gas density, ρ_g	1.225 kg/m^3
Gas viscosity, μ_g	1.8×10^{-5} kg/m·s
Flow condition	
Mass loading	0.5
Gravity, $\vec{g}$	$[-9.81, 0, 0]$ m/s^2

The implemented boundary conditions correspond to the parameters from the experimental campaign carried out by Bohnet and Triesch (2003). A uniform velocity magnitude (25 m/s), solids volume fraction of 2.45×10^{-4} (equivalent to a mass-loading of 0.5) and turbulence intensity of 0.1% were specified at the gas inlet boundary. These inlet values are expected to develop throughout the pipe of length L_1, all the way to the diffuser entrance. Zero-pressure gradient was specified at the outlet boundary. The partial-slip wall boundary conditions proposed by Johnson and Jackson (1987) were specified for the solids phase in the TFM. Following recommendations of previous studies (Benavides & van Wachem, 2008; Li et al., 2014; Shah et al., 2015), a specularity coefficient much less than 1 was chosen. Hybrid initialization was used to initialize the flow variables.

Table 2 Modeling parameters and simulation settings

Parameter	Value/scheme used
e_s	0.9
e_w	0.95
φ	0.1
Packing limit, $\phi_{s,\max}$	0.63
Pressure-velocity coupling	Coupled
Pressure discretization	PRESTO
Momentum discretization	QUICK
Volume fraction discretization	QUICK
Turbulence discretization	QUICK
Granular temperature	QUICK
Flow Courant number	10
Explicit relaxation of pressure and momentum	0.75
Unsteady formulation	First-order implicit
Convergence criteria	10^{-4}
Time step	0.001 s

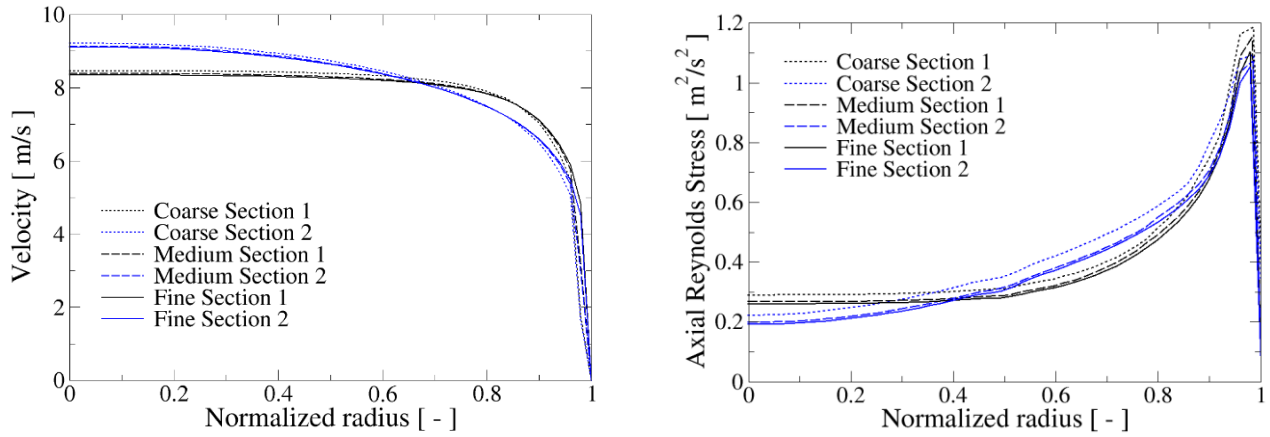

(a) Axial velocity (b) Axial Reynolds Stress

Fig. 2 Grid independence analysis for the three grids considered in this work

Table 3 Mesh study with three different grid sizes

		Average Relative Error [%]			
Grid	Size (cells)	Axial Velocity S1	Axial Velocity S2	Axial Stress S1	Axial Stress S2
Coarse	$\approx 5 \cdot 10^5$	2.57	2.31	3.49	4.81
Medium	$\approx 2 \cdot 10^6$	1.11	0.97	1.03	2.47
Fine	$\approx 4 \cdot 10^6$	–	–	–	–

3.2 Grid Convergence Analysis

Three structured grids, namely, coarse, medium and fine, are used for the grid sensitivity analysis. The profiles of velocity and axial Reynolds stresses in sections 1 and 2 have been taken as the objective functions. Figure 1 show the axial velocity profiles in both sections, where it is noticeable how the curves of medium and fine grids are nearly superimposed. Same comments are valid for the axial stresses.

As a measure to quantify the difference between the corresponding profiles, the average relative error ε regarding the fine grid is introduced by the following expression:

$$\varepsilon = \frac{1}{N}\sum_{i=i}^{N}\left|\frac{\phi_{i,g}-\phi_{i,fine}}{\phi_{i,fine}}\right| \quad (8)$$

Where $\phi_{i,g}$ is the relevant variable (axial velocity or stress) in the grid g (coarse or medium) evaluated in the i point of the curve. Here, each curve has been built based on fifty points (N = 50). The average relative error for each of the four curves is found in Table 3.

As it can be seen the maximum differences between the medium and fine grid are around 1% in the velocity profiles and 2.5% in the axial stress profiles, so the solution for the clean flow can be considered as grid independent. Nevertheless, to keep the highest possible accuracy, the two-phase computations have been performed in the fine grid, which did not imply an excessive computational time in the available hardware.

4. Results and Discussion

A direct comparison with experimental measurements and an interpretation of the physics observed in the simulation results are presented in this section, together with the EL results of De Souza et al. (2014) based on the two-layer k-ϵ turbulence model. Figure 3 shows the gas velocity profiles for the two measuring sections, i.e. $x_1 = 0.7$ m (Fig. 3a) and $x_2 = 2.2$ m (Fig. 3b) downstream the diffuser inlet. The curves obtained in this work are labeled according to the approximations employed and are listed in the figure captions. At the first section $x_1 = 0.7$ m, it is seen that the present single phase flow (SPF) computations are able to capture quite approximately the experimental points (in case of De Souza et al. (2014), not shown, the SPF gas velocity is over-predicted). At section $x_2 = 2.2$ m, the central value of gas velocity is under-predicted which was also the case in De Souza et al. (2014) and in Bohnet and Triesch (2003) (not shown). In the case of two-phase flow, the present Euler-Lagrange computations and those of De Souza et al. (2014) under-predict the gas phase velocity; however, both describe correctly the qualitative modifications of the gas flow by particles: in section 1 the gas is accelerated and in section 2 it is decelerated. On the other hand, the TFM computations over-predict the loaded case gas velocity in the center in section 1, but in section 2 the KTGF is the only model able to capture the gas centerline velocity; when the granular temperature equation is not considered the velocity profile is pretty close to the EL simulations.

The higher values of gas velocity provided by the TFM-KTGF approach are explained in Fig. 4, showing the profiles of solids velocity at the two sections. Unfortunately, Bohnet and Triesch (2003) do not report measurements of any variable related to the particles. From the graphs in Fig. 4, it can be observed that such TFM-KTGF model generates the largest values for the solids velocity in both sections which are above the gas velocity. Therefore, the solids phase accelerates the continuous phase rendering higher values of its velocity

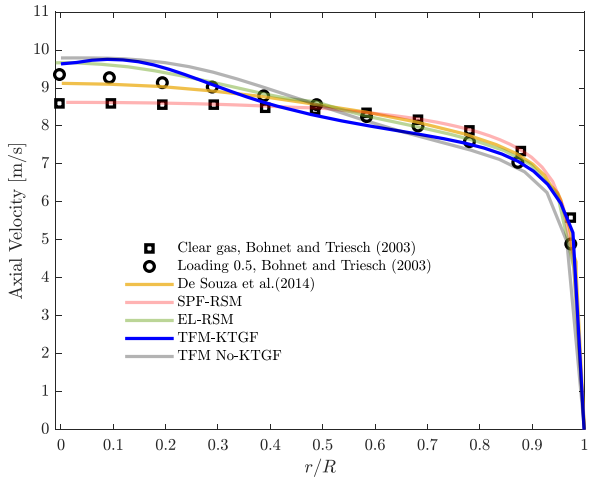

(a) Section $x_1 = 0.7$ m

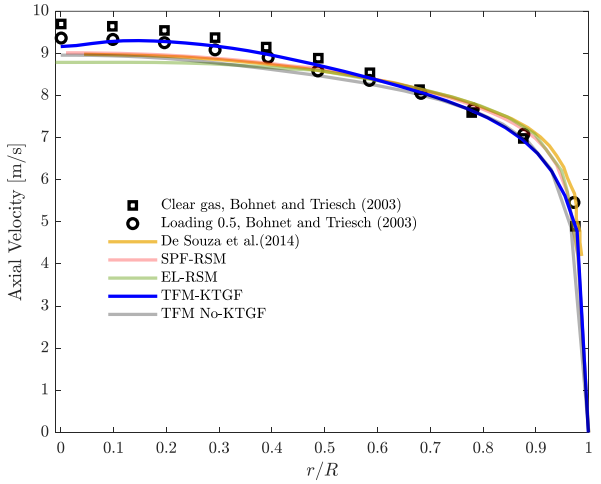

(b) Section $x_2 = 2.2$ m

Fig. 3 Gas phase axial velocity profiles; SPF = single phase flow; EL = Euler-Lagrange; RSM = Reynolds Stress Model; TFM = two-fluid model; KTGF = kinetic theory of granular flow.

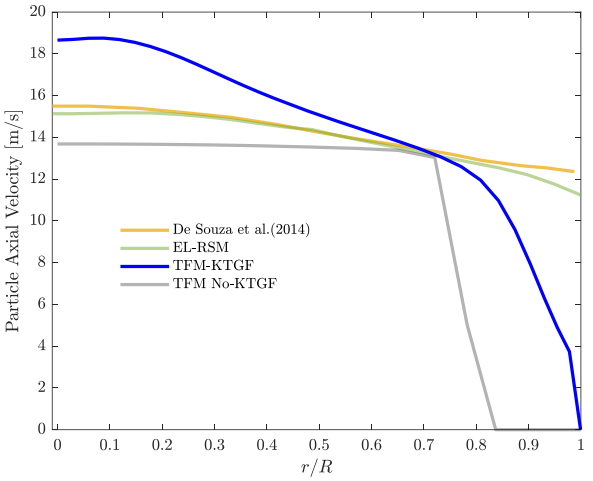

(a) Section $x_1 = 0.7$ m

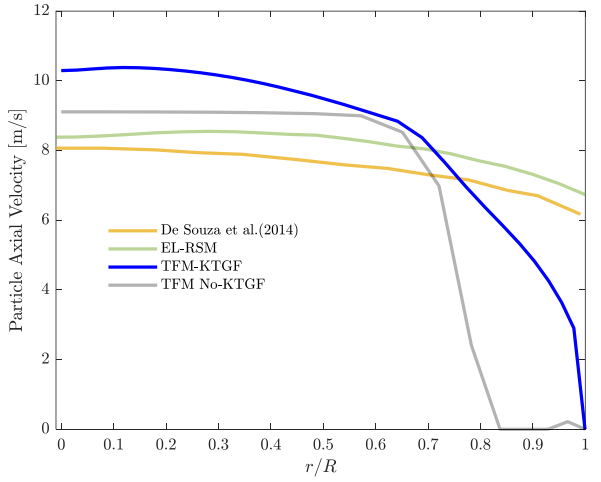

(b) Section $x_2 = 2.2$ m

Fig. 4 Solids phase axial velocity profiles; EL = Euler-Lagrange; RSM = Reynolds Stress Model; TFM = two-fluid model; KTGF = kinetic theory of granular flow.

in the center of the pipe. This phenomenon is due to a reduced spreading of solids velocity across the pipe transversal section. In the case of De Souza et al. (2014), the solids phase velocity in section 1 is similar to that obtained by the present EL computations, both being higher than the fluid velocity. In section 2, particle velocity reported by De Souza et al. (2014) is lower than that of the gas, so at that location particles extract momentum from the gas, reducing its velocity as shown in Fig. 3b. The present EL simulations predict very close velocities for gas and particles in section 2, explaining why gas velocities in single and two-phase flow are pretty close at that location. Regarding the TFM, the case without granular temperature, TFM No-KTGF, the solids velocity profile does not show any appreciable spreading so particles tend to follow straight trajectories; the TFM-KGTF, on the other hand, shows a certain spreading of the solids phase mean velocity along the cross-section but lower than the EL computations. In this last case, solids velocities in the pipe centerline are remarkably higher than those predicted by the other approaches.

The gas phase streamwise turbulent intensity $u_g{}'$ (computed as the square root of axial normal Reynolds Stress over the fluid mean velocity in the outlet pipe) in the two sections downstream the diffuser is presented in Fig. 5. As for this variable, De Souza et al. (2014) did not provide values, only the present computations are compared versus the experimental results. In single-phase flow, SPF, the Reynolds Stress Model is able to provide results of $u_g{}'$ which compare well with the measurements, although its centerline values in section 2 are slightly overpredicted. For two-phase flow, at the two considered sections, the TFM provides profiles of $u_g{}'$ that are above the experimental results for both cases, using or not the granular temperature equation, being clearly higher than measurements in section 1. The TFM-KTGF curve does not reproduce the peak of $u_g{}'$ observed by the experiments close to the wall in both sections; however, the No-KTGF results do show such a trend, which is seen clearly in section 2 (Fig. 5b). This fact is due to an excessive prediction of particle spreading by the KTGF model so that particles close to the wall damp gas fluctuations in that area. Qualitatively the TFM profiles reproduce the turbulence enhancement in two-phase flow regarding SPF in section 1 but fail to describe the turbulence attenuation due to particles in section 2.

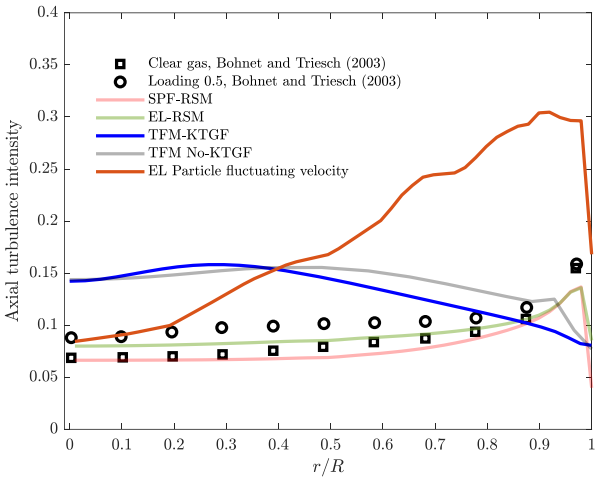

(a) Section $x_1 = 0.7$ m

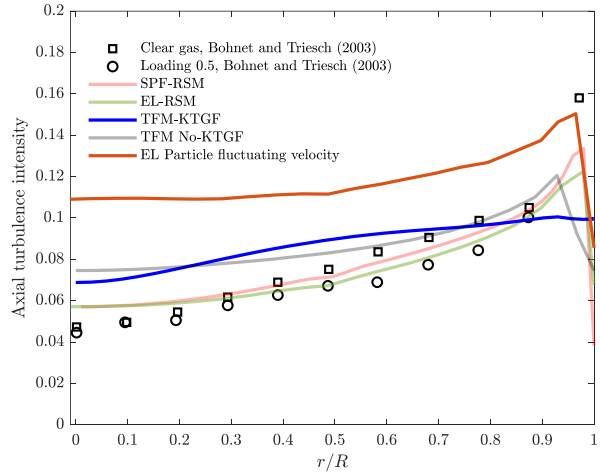

(b) Section $x_2 = 2.2$ m

Fig. 5 Streamwise turbulence intensity downstream the diffuser; SPF = single phase flow; EL = Euler-Lagrange; RSM = Reynolds Stress Model; TFM = two-fluid model; KTGF = kinetic theory of granular flow.

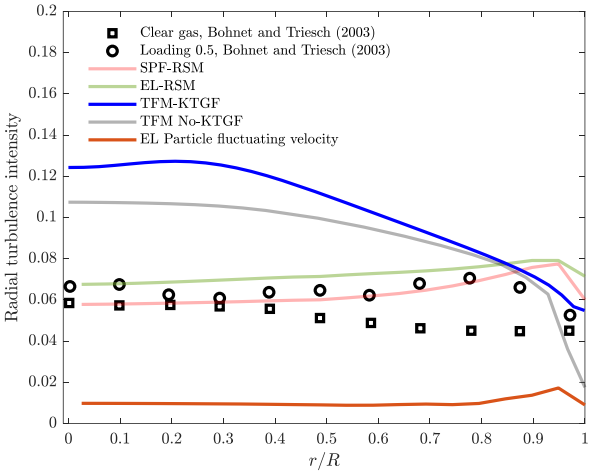

(a) Section $x_1 = 0.7$ m

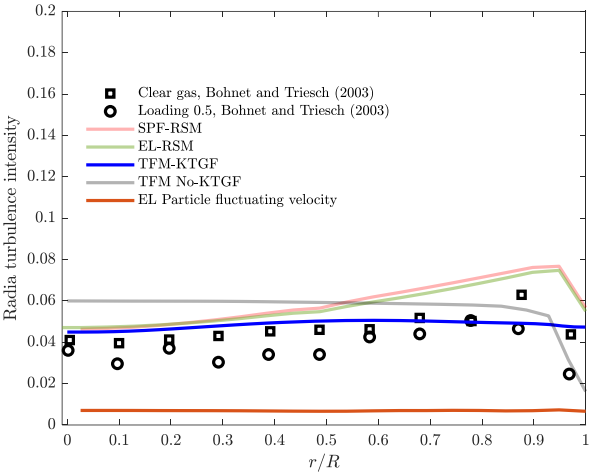

(b) Section $x_2 = 2.2$ m

Fig. 6 Radial turbulence intensity downstream the diffuser; SPF = single phase flow; EL = Euler-Lagrange; RSM = Reynolds Stress Model; TFM = two-fluid model; KTGF = kinetic theory of granular flow.

Regarding the EL results in laden flow, they tend to reproduce fairly well the trends of $u_g{}'$ in experiments in the two analyzed sections. The observed peak near the wall is captured and also the right direction of turbulence modification; in section 1, the loaded curve is above the SPF, although it is slightly lower than the experiments. In section 2 the unloaded and loaded gas $u_g{}'$ profiles are over-imposed in the pipe centerline, as in the experiments; however, in this area, numerical curves are slightly higher than the measured points. The EL two-phase flow gas curve remains close and below the SPF, which overpredicts the measurements in this case but it keeps the qualitative behavior that turbulence is damped by particles in this section 2. Finally, although there are no measurements, the particle axial turbulence intensity is included in Fig. 5 which is higher than that of the fluid.

Figure 6 displays the radial turbulence intensity $v_g{}'$ of gas and particles (the last ones obtained in the EL simulation) in the two sections downstream of the diffuser. $v_g{}'$ is defined in the same way as $u_g{}'$ in Fig. 5. The SPF computations with the Reynolds Stress Model, capture well the values of $v_g{}'$ near the center of the pipe in both sections but overpredict it close to the wall. Regarding the two-phase flow, both versions of TFM deliver noticeably higher values for the radial turbulence intensity than EL computations in section 1, similar to what happens with the axial intensity. Therefore, compared with the experiments, the TFM overestimates the kinetic turbulent energy k; however, the EL prediction is close to the measurements, providing a better estimation of k. In section 2, the trend is changed, and the TFM profiles are closer to the experimental points than the EL curves, which are moderately over them. Another difference is that the curves of $v_g{}'$ in section 2 of TFM are flatter than those of EL, which display a characteristic peak near of the wall, similar to experiments. Also, it is remarkable that TFM-KTGF and EL approaches describe qualitatively well the turbulence modification in the radial direction by particles at the two considered downstream locations, enhancing it in section 1 and damping it in section 2. Finally, the corresponding profiles for the particles $v_s{}'$ are shown in Fig. 6, which are much smaller than the solids' axial turbulence intensity, a fact also observed in Laín et al. (2023) in particle laden turbulent channel flow; the computed

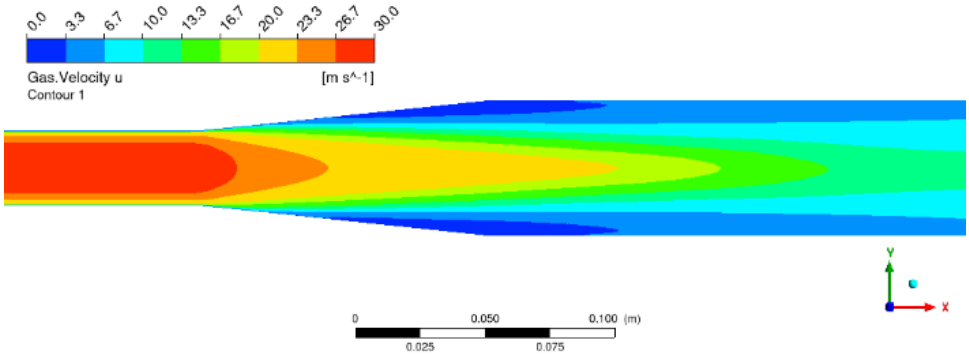

(a) Gas phase velocity

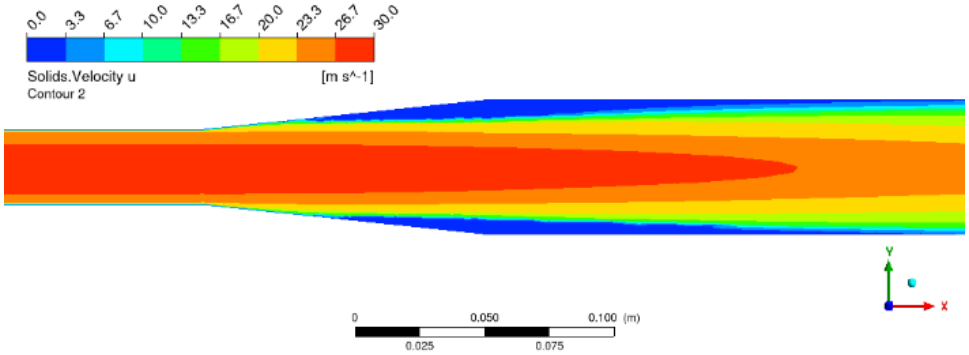

(b) Solids phase velocity

Fig. 7 Velocity contours at the center plane

Table 4 Estimation of the pressure recovery coefficient

Model	C_p
SPF-RSM	0.7842
EL-RSM	0.8375
TFM-KTGF	0.6081
TFM No-KTGF	0.7978
Ideal performance	0.9055
Empirical correlation	0.8057

particle velocity fluctuations present flat profiles in the analyzed sections.

Figure 7 displays contour plots of the two-phase flow gas (Fig. 7a) and particles (Fig. 7b) velocity fields predicted by the TFM-KTGF in the zone around the diffuser. In such figures, it can be seen that the fully developed gas flow enters the diffuser and, due to mass conservation, the velocity field tends to spread quickly showing, near the diffuser wall, zones with very low velocity. However, the flow field is not separated from the wall, which agrees with the known fact that particles tend to avoid such flow detachment in diffusers (Kale & Eaton, 1985; De Souza et al., 2014). The gas and solids velocity contours shown in Fig. 7 are symmetric, contrary to the velocity profiles reported by Chou and Liao (2023) which are skewed due to the presence of a recirculation zone as a result of a higher diffuser angle. The absence of flow separation leads to levels of pressure recovery closer to the ideal performance. Estimates of C_p by the different modeling approaches are summarized in Table 4. It is worth noting the similarity between the C_p obtained from the SPF-RSM simulation and the value calculated with an empirical correlation (Rennels & Hudson, 2012) for single phase flow. The EL-RSM approach shows a significant enhancement in pressure recovery due to the presence of particles while the TFM No-KTGF approach shows a slight increment in C_p compared to the SPF-RSM result. On the other hand, the TFM-KTGF simulation predicts a drop in C_p in particle-laden flow. This opposite trend can be attributed to the turbulence enhancement in the diffuser, due to the transfer of fluctuating kinetic energy from the solids phase. This mechanism is not present in the TFM No-KTGF simulation. Regarding the solids (Fig. 7b), as the flow is vertical and particles are quite inertial, they tend to follow mean straight trajectories and their velocity field shows a sort of block profile that slowly spreads towards the walls, eventually producing flatter profiles downstream the diffuser, like those shown in Fig. 4. This behavior of the particles accelerates the fluid and also is responsible for the increase of fluid turbulence observed in section 1 (Fig. 3a and Fig. 5a).

Figure 8 shows the contours of gas kinetic energy (Fig. 8a) and solids granular temperature (Fig. 8b) in the two-phase flow provided by the TFM-KTGF approach. From Fig. 8a, it is clearly seen how two high k zones (corresponding to a ring in the pipe) are generated at the

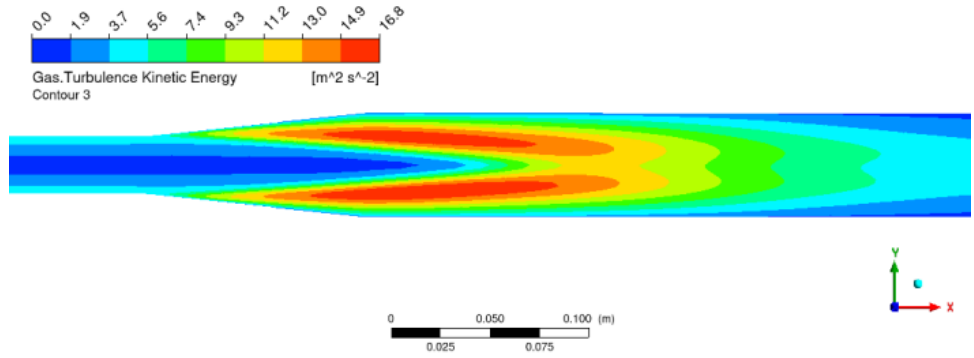

(a) Turbulent kinetic energy

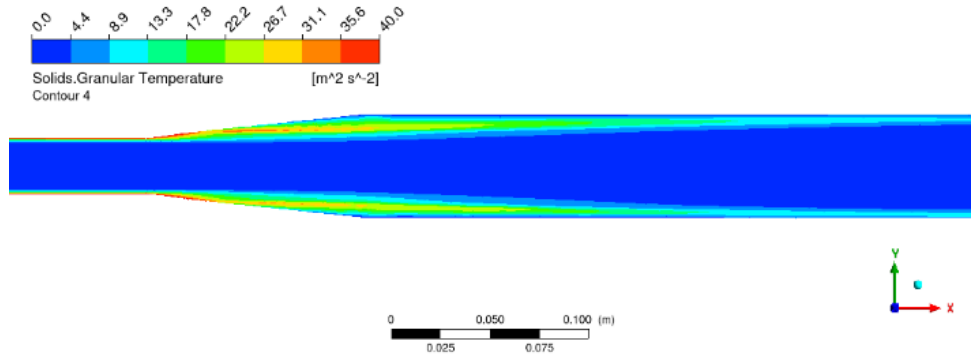

(b) Granular temperature

Fig. 8 Contours of gas phase and solids phase fluctuating energy at the center plane

diffuser entrance, mainly due to the appearance of the velocity gradients in the expansion which generate the shear responsible for turbulent kinetic energy production. Such high k areas beyond the diffuser exit are bent toward the pipe center with the effect of diffusing and spreading the Reynolds Stress profiles seen in Fig. 5. Regarding the granular temperature, Fig. 8b shows how this quantity is generated in the zone close to the diffuser walls, where solid phase shear is high, reaching values more than twice the gas fluctuating energy but keeping low at the pipe centerline. Such areas of high Θ_s spread slowly downstream the diffuser tending to produce fairly uniform values at long enough distances. Actually, the high values of Θ_s within the diffuser are responsible for the high values of $u_g{}'$ seen in Fig. 5a in the TFM simulation; fluctuating energy transfer to the continuous phase is boosted by the modulation term Π_k in Eq. (5).

5. CONCLUSION

A computational study of the turbulent gas-solid flow in a 12° conical diffuser has been conducted using both the Two-Fluid Model (TFM) and the Euler-Lagrange (EL) frameworks. The TFM incorporates closures from the kinetic theory of granular flow (KTGF) and the Reynolds Stress Model (RSM) is used to account for turbulence in both modeling approaches. Simulations are performed in the commercial CFD software ANSYS-Fluent 2022-R2. A unique particle diameter of 150 μm is used to characterize the solids phase. Gas axial velocity profiles are compared with experimental benchmark data and simulation results reported by other researchers. The comparison is drawn at two sections (section 1 at $x_1 = 0.7$ m and section 2 at $x_2 = 2.2$ m) downstream of the diffuser inlet. Single-phase flow (SPF) computations are in good agreement with the experimental profiles reported by Bohnet and Triesch at the analyzed downstream positions. Results from the two-phase flow simulations correctly capture the gas acceleration and deceleration in sections 1 and 2, respectively. The axial gas velocity profiles obtained from the EL simulations of this work agree with those reported by De Souza. The solids velocity is higher than the gas velocity in section 1, which is also in agreement with the results of De Souza, however, the TFM-KTGF predicts rather high values of solids velocity toward the centerline of the pipe in both sections. It can be attributed to a reduced spreading of solids across the pipe transversal section, i.e. particles tend to follow straight trajectories.

The present work highlights the computation of streamwise and radial turbulence intensity in a conical diffuser, which is a subject that has not been fully addressed in previous investigations. The numerical results demonstrate that the incorporation of a solids phase, modeled either as a continuum or a group of particle parcels, has a significant effect on the gas phase velocity fluctuations even at relatively low solids volume fractions. Results of streamwise and radial turbulence

intensity obtained from EL and TFM simulations are compared with the experimental data of Bohnet and Triesch in sections 1 and 2. Only the EL model is able to reproduce the correct trend of turbulence enhancement (section 1) and attenuation (section 2) in the streamwise and radial directions, which reflects the necessity of improving some TFM closures. It is found that turbulence modulation has a significant effect on the predicted pressure recovery in the diffuser. The EL-RSM approach predicts an additional pressure recovery of 6.8% due to the sole presence of the solids phase. Profiles of turbulence intensity reveal that particle velocity fluctuations are more intense in the streamwise direction as was observed in channel flow (Laín et al., 2023). On the other hand, the interphase turbulence modulation terms in the TFM generate too much turbulent kinetic energy. Possible future extensions of this work include the use of a more sophisticated turbulence model, i.e. LES, within the EL framework to resolve relevant flow scales in the diffuser and account for their effect on the particle motion. Various particle sizes and a polydispersed distribution could also be investigated with the EL approach. Regarding the TFM framework, more effort should be put into the modeling of the solids phase shear stress tensor to account for the effect of interstitial fluid on the momentum flux. Turbulence modulation terms should be adjusted to account for the right transfer of turbulent kinetic energy between gas and solids phases. These adjustments in the TFM approach may lead to more reliable predictions of particle-laden flows in the presence of adverse pressure gradients.

ACKNOWLEDGEMENTS

We acknowledge the use of the ANSYS License and computational resources provided by the Department of Mechanical and Mechatronics Engineering at Universidad Nacional de Colombia, sede Bogotá.

CONFLICT OF INTEREST

The authors declare that they have no competing interests.

AUTHORS CONTRIBUTION

A. Benavides-Moran: Conceptualization, methodology, data collection, validation, formal analysis, writing and editing the original draft. S. Lain: conceptualization, methodology, data collection, manuscript revision.

REFERENCES

Ansys (2022). *Ansys Fluent Theory Guide, Release 2022-R2*.

Benavides, A., & van Wachem, B. (2008). Numerical simulation and validation of dilute turbulent gas-particle flow with inelastic collisions and turbulence modulation. *Powder Technology*, *182*(2), 294-306. https://doi.org/10.1016/j.powtec.2007.06.028

Benavides, A., & van Wachem, B. (2009). Eulerian-eulerian prediction of dilute turbulent gas-particle flow in a backward-facing step. *International Journal of Heat and Fluid Flow*, *30*(3), 452-461. https://doi.org/10.1016/j.ijheatfluidflow.2009.02.012

Bohnet, M., & Triesch, O. (2003). Influence of particles on fluid turbulence in pipe and diffuser gas-solids flow. *Chemie-Ingenieur-Technik*, *75*(7), 1254-1261. https://doi.org/10.1002/cite.200300050

Chou, Y. W., & Liao, C. C. (2023). *Numerical simulation of the pneumatic conveying of dilute particulate flows in a diffuser using Euler-Euler approach.* AIP Conference Proceedings, 2685. https://doi.org/10.1063/5.0112082

Crowe, C. T., Schwarzkopf, J. D., Sommerfeld, M., & Tsuji, Y. (2011). *Multiphase flows with droplets and particles*. 2nd ed., CRC Press.

De Souza, F. J., Silva, A. L., & Utzig, J. (2014). Four-way coupled simulations of the gas-particle flow in a diffuser. *Powder Technology*, *253*, 496-508. https://doi.org/10.1016/j.powtec.2013.12.021

El-Askary, W. A., Ibrahim, K. A., El-Behery, S. M., Hamed, M. H., & Al-Agha, M. S. (2015). Performance of vertical diffusers carrying Gas-solid flow: Experimental and numerical studies. *Powder Technology*, *273*, 19-32. https://doi.org/10.1016/j.powtec.2014.12.023

Johnson, P. C., & Jackson, R. (1987). Frictional-collisional constitutive relations for granular materials, with application to plane shearing. *Journal of Fluid Mechanics*, *176*, 67-93. https://doi.org/10.1017/S0022112087000570

Kale, S. R., & Eaton, J. K. (1985). An experimental investigation of gas-particle flows through diffusers in the freeboard region of fluidized beds. *International Journal of Multiphase Flow*, *11*(5), 659-674. https://doi.org/10.1016/0301-9322(85)90085-0

Laín, S., Ortíz, D., Ramírez, J. A., & Duque, C. A. (2023). Analysis and discussion of two-way coupling effects in particle-laden turbulent channel flow. *Ingenieria e Investigacion*, *43*(1), e87275. https://doi.org/10.15446/ing.investig.87275

Laín, S., & Sommerfeld, M. (2007). A study of the pneumatic conveying of non-spherical particles in a turbulent horizontal channel flow. *Brazilian Journal of Chemical Engineering*, *24*(4), 535-546. https://doi.org/10.1590/S0104-66322007000400007

Laín, S., & Sommerfeld, M. (2013). Characterisation of pneumatic conveying systems using the Euler/Lagrange approach. *Powder Technology*, *235*, 764-782. https://doi.org/10.1016/j.powtec.2012.11.029

Laín, S., Sommerfeld, M., & Kussin, J. (2002). Experimental studies and modelling of four-way

coupling in particle-laden horizontal channel flow. *International Journal of Heat and Fluid Flow*, *23*(5), 647-656. https://doi.org/10.1016/S0142-727X(02)00160-1

LaMarche, C. Q., Morán, A. B., van Wachem, B., & Curtis, J. S. (2017). Two-fluid modeling of cratering in a particle bed by a subsonic turbulent jet. *Powder Technology*, *318*, 68-82. https://doi.org/10.1016/j.powtec.2017.05.008

Li, T., Gel, A., Pannala, S., Shahnam, M., & Syamlal, M. (2014). CFD simulations of circulating fluidized bed risers, part I: Grid study. *Powder Technology*, *254*, 170-180. https://doi.org/10.1016/j.powtec.2014.01.021

Lun, C. K. K., Savage, S. B., Jeffrey, D. J., & Chepurniy, N. (1984). Kinetic theories for granular flow: Inelastic particles in Couette flow and slightly inelastic particles in a general flowfield. *Journal of Fluid Mechanics*, *140*, 223-256. https://doi.org/10.1017/S0022112084000586

Rennels, D. C., & Hudson, H. M. (2012). *Pipe flow: A practical and comprehensive guide*. https://doi.org/10.1002/9781118275276

Schut, S. B., Van Der Meer, E. H., Davidson, J. F., & Thorpe, R. B. (2000). Gas-solids flow in the diffuser of a circulating fluidised bed riser. *Powder Technology*, *111*(1–2), 94-103. https://doi.org/10.1016/S0032-5910(00)00245-X

Senapati, S. K., & Dash, S. K. (2021). Gas–solid flow in a diffuser: Effect of inter-particle and particle–wall collisions. *Particuology*, *57*, 187-200. https://doi.org/10.1016/j.partic.2021.01.006

Shah, M. T., Utikar, R. P., Pareek, V. K., Tade, M. O., & Evans, G. M. (2015). Effect of closure models on Eulerian-Eulerian gas-solid flow predictions in riser. *Powder Technology*, *269*, 247-258. https://doi.org/10.1016/j.powtec.2014.08.064

Viollet, P. L. & Simonin, O. (1994). Modelling Dispersed Two-Phase Flows: Closure, Validation and Software Development. *ASME Applied Mechanics Reviews* 47(6S): S80–S84.

Sinclair, J. L., & Jackson, R. (1989). Gas-particle flow in a vertical pipe with particle-particle interactions. *AIChE Journal*, *35*(9). 1473-1486. https://doi.org/10.1002/aic.690350908

Speziale, C. G. (1995). *A Review of Reynolds Stress Models for turbulent shear flows*. 20th Symposium On Naval Hydrodynamics, National Acadmic Press.

Syamlal, M., Rogers, W., & O`Brien, T. J. (1993). *MFIX documentation theory guide*. https://doi.org/10.2172/10145548

Triesch, O., & Bohnet, M. (2001). Measurement and CFD prediction of velocity and concentration profiles in a decelerated gas-solids flow. *Powder Technology*, *115*(2). 101-113. https://doi.org/10.1016/S0032-5910(00)00337-5

Wen, C. Y., & Yu, Y. H. (1966). Mechanics of fluidization. *Chemical Engineering Progress, Symposium Series*, *62*(1). 100-111.

APPENDIX

Table A1. Constitutive relations of the TFM

- Laminar flow stress tensor:

$$\mathcal{T}_g = \mu_g \left[\nabla\vec{V}_g + \left(\nabla\vec{V}_g\right)^T - \tfrac{2}{3}(\nabla\cdot\vec{V}_g)\mathcal{I}\right] \quad \text{(A1)}$$

- Solids phase stress tensor:

$$\mathcal{T}_s = \mu_s\left(\nabla\vec{V}_s + \nabla\vec{V}_s^T\right) - \left(\lambda_s - \tfrac{2}{3}\mu_s\right)(\nabla\cdot\vec{V}_s)\mathcal{I} \quad \text{(A2)}$$

- Solids phase pressure and bulk viscosity (Lun et al., 1984):

$$P_s = \phi_s\rho_s\Theta_s + 2\rho_s(1+e_s)\phi_s^2 g_0\Theta_s \quad \text{(A3)}$$

$$\lambda_s = \tfrac{4}{3}\phi_s^2\rho_s d_s g_0(1+e_s)\sqrt{\tfrac{\Theta_s}{\pi}} \quad \text{(A4)}$$

- Solids shear viscosity and conductivity (Syamlal et al., 1993):

$$\mu_s = \tfrac{d_s\rho_s\sqrt{\pi\Theta_s}}{6(3-e_s)}\left[1+\tfrac{2}{5}\phi_s g_0(1+e_s)(3e_s-1)\right] \quad \text{(A5)}$$

$$\kappa_s = \tfrac{15\rho_s d_s n\phi_s^2 g_0\sqrt{\pi\Theta_s}}{4(41-33n)}\left[1+\tfrac{12}{5}n(4n-3)+\tfrac{16}{15\pi}(41-33n)\right] \quad \text{(A6)}$$

With $n = \frac{1}{2}(1+e_s)$

- Radial distribution function (Sinclair & Jackson, 1989):

$$g_0 = \left[1-\left(\frac{\phi_s}{\phi_{s,\max}}\right)^{1/3}\right]^{-1} \quad \text{(A7)}$$

- Collisional dissipation of Θ_s (Lun et al., 1984):

$$\gamma_s = \tfrac{12(1-e_s^2)g_0}{d_s\sqrt{\pi}}\rho_s\phi_s^2\Theta_s^{3/2} \quad \text{(A8)}$$

- Interphase momentum transfer coefficient:

$$\beta_{sg} = \tfrac{3}{4}C_D\tfrac{\phi_s\rho_g|\vec{V}_s-\vec{V}_g|}{d_s(1-\phi_s)^{1.65}} \quad \text{(A9)}$$

Where the drag coefficient for dilute flow is modeled according to Wen & Yu (1966):

$$C_D = \tfrac{24}{(1-\phi_s)Re_s}(1+0.15\cdot[(1-\phi_s)Re_s]^{0.687}) \quad \text{(A10)}$$

Where $Re_s = \frac{\rho_g d_s|\vec{V}_s-\vec{V}_g|}{\mu_g}$

Table A2. Turbulence closures

- The turbulence dispersion force is modeled according to (Simonin & Viollet, 1990):

$$\vec{F}_{td} = -k_{sg}\vec{V}_{dr} \quad \text{(A11)}$$

Where the covariance of gas phase and solids phase velocity fluctuations is $k_{sg} = 2k\left(\frac{\chi+\eta}{1+\eta}\right)$, with $\chi =$

$(1 + C_v)\left(\frac{\rho_s}{\rho_g} + C_v\right)^{-1}$ and $\eta = \frac{\tau_{t,sg}}{\tau_{F,sg}}$. The drift velocity is $\vec{V}_{dr} = -\frac{\mathcal{D}_{sg}}{\sigma_{sg}}\left(\frac{1}{\phi_s}\nabla\phi_s - \frac{1}{\phi_g}\nabla\phi_g\right)$ with $\mathcal{D}_{sg} = \frac{1}{3}k_{sg}\tau_{t,sg}$.

- The Lagrangian integral time-scale calculated along particle trajectories is:

$$\tau_{t,sg} = \frac{\tau_{t,g}}{\sqrt{1+C_\beta\xi^2}} \quad \text{(A12)}$$

With $C_\beta = 1.8 - 1.35\cos^2\theta_t$ and $\xi = \frac{|\vec{V}_g - \vec{V}_s|\tau_{t,g}}{L_{t,g}}$. θ_t is the angle between the mean particle velocity and the mean relative velocity.

- Particle relaxation time due to inertial effects acting on the solids phase:

$$\tau_{F,sg} = \frac{\phi_s\rho_s}{\beta}\left(\frac{\rho_s}{\rho_g} + C_v\right) \quad \text{(A13)}$$

- Characteristic turbulent time-scale:

$$\tau_{t,g} = \frac{3}{2}C_\mu\frac{k}{\epsilon} \quad \text{(A14)}$$

- Characteristic turbulent length-scale:

$$L_{t,g} = \sqrt{\frac{3}{2}}C_\mu\frac{k^{3/2}}{\epsilon} \quad \text{(A15)}$$

- Turbulent viscosity:

$$\mu_t = \rho_g C_\mu\frac{k^2}{\epsilon} \quad \text{(A16)}$$

- Turbulence modulation term due to the solids phase:

$$\Pi_k = \beta_{sg}\left[k_{sg} - 2k - \left(\vec{V}_g - \vec{V}_s\right)\cdot\vec{V}_{dr}\right] \quad \text{(A17)}$$

- Modulation effect of the solids phase on the dissipation rate equation:

$$\Pi_\epsilon = C_{\epsilon,3}\frac{\epsilon}{k}\Pi_k \quad \text{(A18)}$$

- Turbulence model constants:

$C_{\epsilon.1} = 1{,}44,\ C_{\epsilon.2} = 1{,}92.\ C_{\epsilon.3} = 1{,}2.\ \sigma_{sg} = 0{,}75$

$C_v = 0{,}5.\ C_\mu = 0{,}09.\ \sigma_\epsilon = 1{,}3$